https://doi.org/10.1016/j.cad.2023.103517

OPS-ITO: Development of Isogeometric Analysis and Topology Optimization in OpenSEES for free-form structural design

Zixin Zhang[1,2], Liming Jiang[1,2,*], Tejeswar Yarlagadda[1], Yao Zheng[3], Asif Usmani[1,2]

[1] *Department of Building Environment and Energy Engineering, The Hong Kong Polytechnic University, Hung Hom, Hong Kong SAR*

[2] *Research Institute for Sustainable Urban Development, The Hong Kong Polytechnic University, Hung Hom, Hong Kong SAR*

[3] *School of Aeronautics and Astronautics, Zhejiang University, Zhejiang, China*

Abstract: Unlike the current design routine manually defining geometries for computational analyses, a future-oriented computer-aided design tool can generate a structural model through automated model optimization and iterative analyses. The topology optimization technique uses elemental density variables to formulate a computationally varying model based on analysis results, while an isogeometric analysis could facilitate the automatic iteration without adapting the mesh scheme at each step. This paper aims to bring these capabilities in the open-source simulation platform OpenSEES. The IGAQuad and IGABrick elements using NURBS based shape functions and geometric description are developed in this widely-used finite element modelling framework, which are then ported to a density-based topology optimization module. The modelling capabilities of the IGA elements have been verified using classic problems. The model optimization processes for loaded structural members are demonstrated using 2D and 3D cases, in which the eventually obtained geometric models are fundamentally different from the original boxy shapes but of less material cost and comparable structural performance. Although the development in this paper remains limited, the open-source and modular code infrastructure of OpenSees could facilitate continuous development on the basis of the topology optimization and isogeometric analysis in this paper, aiming for a computational tool to synergize the free form structural design and the advanced construction technologies.

Keywords: structural design, open-source software, isogeometric analysis, topology optimization, OpenSEES

1. Introduction

In the conventional design framework for building structures, regular sections were usually presumed and computer-aided structural analyses were only conducted for performance evaluation to comply with code requirements. This design routine has worked efficiently with the widely used steel structures and reinforced concrete structures employing regular structural sections. In a modern design practice, architecture designs adopting a parametric design approach have fascinated the stakeholders by the creative forms, which are particularly represented by Hadid's iconic architecture projects including the Jockey Club building in Hong Kong (as shown in Fig.1). In the practice of structural design, such attempts remain limited, but a great potential has emerged since the introduction of 3D printing technology and prefabricated construction [1, 2], which have been deemed as promising construction solutions for future to resolve forthcoming labour shortage. While preparing for this shift, the design routine of structures should be reshaped to synergize the free-form construction techniques and to exploit the potential of computer-aided designs. In other words, the design software and methodology should ideally generate a structural form breaking the barriers of regular section shapes or structural grids. Instead of assigning a structural form by structural engineers, the computational algorithms should automatically generate a structural design to enable minimum material usage, maximum structural stiffness, and optimum construction ability.

Computer-aided structural designs [3, 4] in the past were substantially facilitated by the development of the finite element methods (FEM) [5], which enable the discretisation of a structural member or a structural system into a number of finite-size elements (beam-column elements, brick or solid elements) for computational analyses. The geometries of structural models in these analyses are given or specified by the users, whereas the analysis tools do not change the model geometries. To automatically generate an optimal structural form upon computation, the Topology Optimization (TO) approach can be adopted, which was previously

used in the discipline of Aerospace Engineering to obtain ultimately light-wight design of mechanical components. This approach was originally proposed by Bendsøe and Sigmund [6], which has been developed into various optimization methods, such as the density-based method [7], the thickness-based method [8], the level set method [9], and the explicit methods including the Moving Morphable Units method [10] and the Deformable Simplicial Complex method [11, 12]. Among them, the Solid Isotropic Material with Penalization (SIMP) method as a density-based approach has been often used, which effectively describes the model topology using the pseudo-density variables at elements or nodes. The attempts of applying TO approach in the designs of structural members have started, which include the optimisation aiming for maximum load-bearing capacities[13], model manufacturability[14] and aesthetic performance [15], and more recently the construction-oriented consideration of topology optimization [16] by the authors.

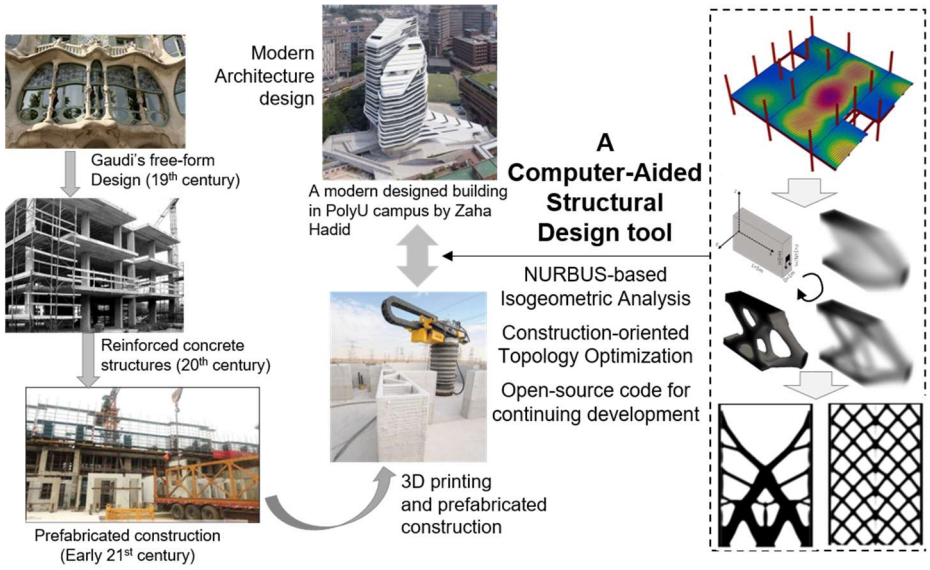

Fig.1 Design tool needed for future free-form structures and construction

The earlier attempts of topology optimization based design obtained an optimal geometry from the automatic iterations using finite element analyses at each optimization step, which is varied by the elemental density variables. A challenge to the finite element model in these analyses is the mesh refinement since the optimized model geometry may be of irregular shapes.

A finite element analysis may easily crash due to the severe stress concertation in the finite elements if maintaining the same mesh scheme. An Isogeometric Analysis (IGA) [17] was developed to the mesh adaptiveness between the analysis models and geometric models [18]. The Isogeometric Analysis proposed by Hughes et al [19] as an extension of conventional FEM, innovatively uses Non-Uniform Rational B-Splines (NURBS) for shape functions instead of linear or polynomial shape functions in finite elements. Moreover, the NURBS shape functions of IGA elements are made identical to the geometry description using NURBS, which seamlessly bridges a computer-aided design (CAD) to a computational analysis model [20, 21]. Moreover, an IGA approach is preferred in topology optimization as the model mesh refinement can be achieved using elevated order of shape continuity (*p-refinement or k-refinement*) without adding additional elements (*h-refinement*) [22-25].

Although topology optimization and isogeometric analyses become key components to potentially realise optimized free-form structural designs and construction, how to implement them in real-scale structural analyses and designs remains a question. Firstly, these components should be integrated into a structural simulation platform of no technical barrier to incorporate continuous development of more optimization algorithms in real-scale design. Secondly, an open-source and object-oriented simulation framework is preferred to ease the burden of developers and the platform should have attracted a number of users and developers [26, 27]. The Open System for Earthquake Engineering Simulation (OpenSEES) is chosen for this long-term task, which is primarily programmed in C++ and interpreted by Tool command language (Tcl) [28] and Python. OpenSees was initially developed in 1990s and has undergone many version iterations with a variety of modelling capabilities [26, 29-31], while the authors of this paper have been deeply involved [32-35] in extending OpenSEES with fire modelling, heat transfer analyses, thermo-mechanical analyses, and integrated analyses with GUIs. The OpenSees codes are of a modular architecture, and a topology optimization module and IGA

elements can be added to exploit the existing modules for materials, analyses, model input and output, etc.

In this paper, an IGAQuad element and an IGABrick element have been developed for 2D analyses and 3D analyses, which enabled the operation of isogemetric analyses in an FEM based simulation framework. The NURBS based model geometry and shape functions have been incorporated into the extended OpenSEES. The computational performance of these IGA elements has been examined using the classic problems, which demonstrates an outstanding capability of dealing with irregular-shape models compared to FEM. The topology optimization module for structural design is developed to integrate the OpenSEES IGA based iterative analyses into the SIMP based topology optimization. The developed codes have been encapsulated as an executable program (namely OPS-ITO) with graphic user interface, which currently offers various constraint functions including the stress limit constraints, minimum width, and objective functions including minimum material consumption, and maximum model stiffness (minimum compliance). The preliminary use of this OPS-ITO platform has been showcased in this paper, while the key steps in future research is to implement more construction-oriented constraints to fulfil the needs of real-scale structural designs co-working with modern construction approaches. The future development could take advantage of this open-source platform as it allows various teams to develop their codes to implement topology optimization in structural designs.

2. Development of Isogeometric Analyses in OpenSEES Framework

2.1 NURBS based Isogeometric Analysis

The NURBS is widely used in CAD to formulate curves, which is also adopted by the IGA for geometry description and shape functions. As one typical form of NURBS, the B-Spline curve is defined using basis functions of a knot vector $\Xi=\left\{\xi_1,\xi_2,...,\xi_{n+p+1}\right\}$, where n and

p are the number of basis functions and the curve order, respectively. The B-Spline curve could be expressed in Cox-de Boor recursive format [36]:

$$
\begin{aligned}
&N_{i,0}(\xi)=\begin{cases}1, \text{ if } \xi_i \le \xi \le \xi_{i+1}\\ 0, \text{ otherwise}\end{cases}\\
&N_{i,p}(\xi)=\frac{\xi-\xi_i}{\xi_{i+p}-\xi_i}N_{i,p-1}(\xi)+\frac{\xi_{i+p+1}-\xi}{\xi_{i+p+1}-\xi_{i+1}}N_{i+1,p-1}(\xi),\\
&\quad (i=1,2,\ldots,n+p+1)
\end{aligned}
\tag{1}
$$

By adding the non-uniform weight values of control points, the NURBS curve is given as:

$$
C(\xi)=\frac{\sum_{i=1}^{n}N_i^p(\xi)\omega_i\mathbf{P}_i}{\sum_{j=1}^{n}N_j^p(\xi)\omega_j}=\sum_{j=1}^{m}R_i^p(\xi)\mathbf{P}_i \tag{2}
$$

Where $\mathbf{P}_i$ and ω_i are the coordinates and weight value of i-th control point, and the p-th order NURBS shape function is labeled as $R_i^p(\xi)$ for simplicity.

For 2D IGA formulation, the shape function using NURBS is described as:

$$
\mathbf{x}(\xi,\eta)=\sum_{i=1}^{n}\sum_{j=1}^{m}R_{i,j}^{p,q}(\xi,\eta)\mathbf{x}_{i,j} \tag{3}
$$

where $R_{i,j}^{p,q}(\xi,\eta)$ is the 2D basis function, and $\mathbf{x}_{i,j}$ represents the variable vectors of the coordinates and displacements. Differing from the conventional finite element approach using isoparametric shape functions, IGA requires two space-mapping processes from the parent space to the parametric space and then to the physical space as illustrated in Fig.2. Therefore, the elemental stiffness matrix of 2D structure is expressed as:

$$
\mathbf{K}_e=\int_{\Omega_e}B^TDB\mathrm{d}\Omega_e=\sum_{i\in\Omega_e}w_iB_i^TDB_i|J_1||J_2|t \tag{4}
$$

Where w_i is the weight value at the i-th gauss integration point, and B_i is the strain-displacement matrix. Here J_2 is the Jacobian matrix of the discrete element domain using gauss integration.

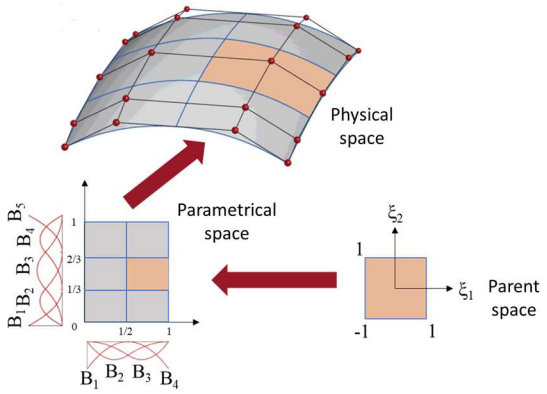

Fig.2 schematic of space-mapping process in Isogeometric analyses

2.2 OpenSEES development for Isogeometric Analysis

OpenSEES is an open-source simulation framework initially developed for finite element analyses of structures subjected to earthquake loading [26], which was later extended by the authors for modelling structures in fires (OpenSEES for fire) [32-35]. Analyses in OpenSEES follow the conventional routine of finite element method, and the simulation process is disseminated into the following common steps: (1) mesh discretization; (2) formulation of stiffness matrices and residual forces in each finite element; (3) assembly of elemental stiffness matrices and force vectors; (4) solving the system of equation; (5) check of convergence and updating elemental state. Taking an object-oriented architecture of source code development, these tasks are conducted in OpenSEES within four basic modules: *ModelBuilder*, *Domain*, *Analysis*, and *Recorder* (blue boxes in Fig.3) along with a variety of supporting packages. The *ModelBuilder* is responsible to building FE models after the mesh discretization, which adds the components of the FE model to the *Domain*. The *Domain* stores the information of an FE model, enabling updates during the FE analysis. As illustrated in Fig.3, the objects of the FE model (green boxes) stored in *Domain* include *Node*, *Material*, *Element*, *Constraint* (single point *SP_Constraint* and multi-point *MP_Constraint,* for boundary conditions), and *LoadPattern* (for imposing various load types). These objects are defined in various projects (modules) as inherited classes taking advantage of the object-oriented nature of C++. When the model is built and stored in *Domain*, finite element analyses can be carried out with the *Analysis*

module, which formulates the global system of equation and solves the equation to obtain converged solution of nodal displacements. To record the analysis results as output, the *recorder* including various recorder objects for nodes and elements are deployed under the request of the user, which retrieves the data from the corresponding model objects.

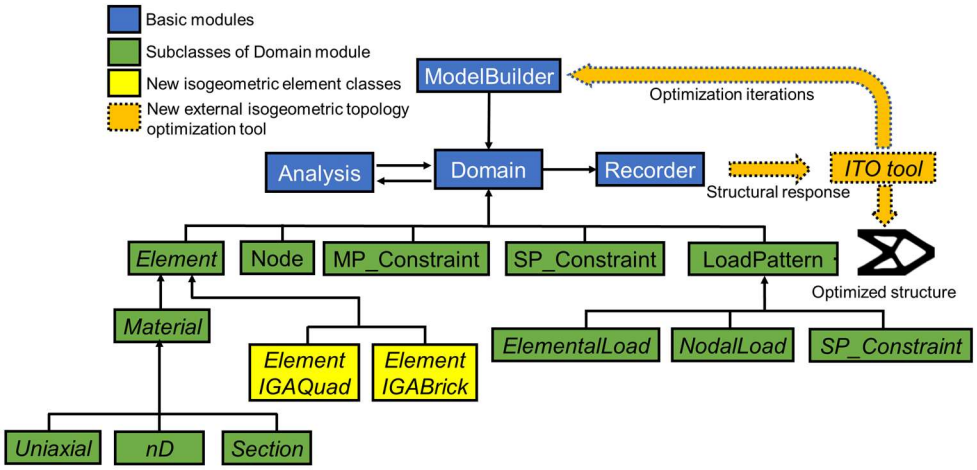

Fig.3 Class hierarchy of OpenSEES framework and ITO extension

The major challenge of developing IGA capability in a FE framework is the different scopes and processes for element definition and state determination. IGA employs NURBS as shape functions with the nodes serving as control points of the splines. The model geometry and shape functions are both described using these splines. As depicted in Fig.3, the new developed IGA element classes are denoted as IGAQuad and IGABrick for 2D and 3D isogeometric analyses, respectively. These elements are to be duplicated as objects and stored in *Domain*, which is now connected to the *ITO tool* package for running topology optimization processes with IGA approach (discussed later). When developing IGA elements in OpenSEES, the interface functions for the computation of characteristic components (e.g., stiffness matrix, load vector, etc) are inherited from the base class of *Element*. The fundamental functions of these interface functions are: (1) to perform in-element interpolation from nodal displacements (NURBS based interpolation in IGA) to section deformation at each integration point; (2) to formulate resisting forces at nodes from the integration of section forces; (3) to formulate element stiffness matrix from the section stiffness matrices. Due to the use of NURBS, these

in-element process (also termed as element state determination) are rewritten with NURBS based interpolation and integration. Noted that more development efforts would be needed for describing complex initial boundary conditions and complex boundary conditions of IGA models. The trimmed surface design method [37] and the isogeometric boundary element method [38] may be helpful to these further developments.

Taking a 2D model as an example, the computation of shape functions for each integration point is conducted within the procedure of *shapeFunction* in the *IGAQuad* element class, which serves as a key step to transform the Isogeometric formulation to standard FE interface of OpenSEES. The work flow of computing the IGA shape function is presented in Fig.4. The knot vector in an IGA element is used to find the belonging knot span of gaussian points for determining the NURBS shape functions (represented by the blue shade) and the Jacobian matrix J_2 for mapping the parent space into parametric space (yellow shade). For each element, the belonging knot span index (*KntSpan*) of each gauss point (*Xg*&*Wg*) is computed from the function *findSpan* [36], which is followed by the calculation of basis function ($N\&dN/d\xi$) for B-Spline (*DerBasisFuns*) and the rationalized $R\&dR/d\xi$. As shown in Fig.4, two steps of space mapping are carried out to compute the corresponding Jacobian matrixes J_1 and J_2 to map the parent space into physical space, which are completed in the function *SpaceMap#1* and *SpaceMap#2*. The stiffness determination is of the similar interface as general FE elements in OpenSEES, whereas the NURBS based shape functions are embedded in calculating the stiffness components and the elemental volume.

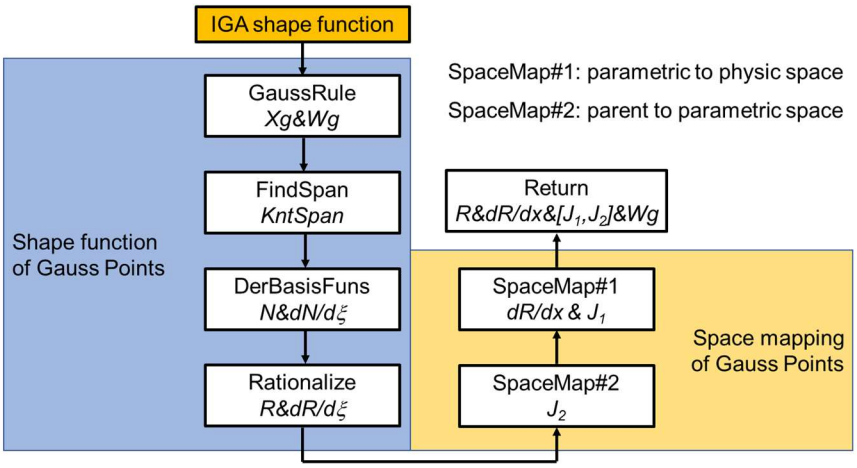

Fig.4 Determination workflow of IGA shape function

2.3 Use of Isogeometric elements in OpenSEES

With the development of IGAQuad and IGABrick elements, isogeometric analyses can be now performed using OpenSEES. The material definition should be specified such as an elastic 2D or 3D material, which is consistent with the original OpenSEES user commands. When using the Python interpreter in OpenSEES, the input command for defining IGAQuad element can be written as follows:

element IGAQuad ex, nex, ey, ney, OrderX, OrderY, CPIds, nKntVectX, KntVectX, nKntVectY, KntVectY, rho_e, WCPs, thk, matTag;

Similarly, the definition script of IGABrick element is in the following form:

element IGABrick ex, nex, ey, ney, ez, nez, OrderX, OrderY, OrderZ, CPIds, nKntVectX, KntVectX, nKntVectY, KntVectY, nKntVectZ, KntVectZ, rho_e, WCPs, matTag

In these command lines, the integers *ex, nex, OrderX* represent the element label, element amount, and element order along the x-direction, respectively, the format of y- and z-direction are in the same manner. *CPIds* is an integer array of the control point label of an element, while the integer *nKntVectX* represents the knot vector length along the *x*-direction (*KntVectX*), likewise in y- and z-direction. The float number *rho_e* is the elemental density that is specially added for the application of topology optimization, which is of a default value of 1. The float number *WCPs* indicate the weight values of each elemental control point, whereas the integer

matTag is the label of applied material. When generating the model using IGA elements in OpenSEES, a more practical approach is to use python-based functions to automatically define the model from the NURBS based geometry. The pre-process is enabled by taking the components from the open-source IGA tool SIMOPackage[39], which has been integrated into the pre-process tool of the topology optimization framework in this paper.

3. Computational performance of Isogeometric Elements in OpenSEES

3.1 2D model: an infinite plate with a circular hole subjected to tension

The first benchmark case of IGA element is to model an infinite plate with a circular hole, which is subjected to constant tension along x axis on both edges as shown in Fig.5. Considering the symmetry, this infinite plate can be simplified as a quarter plate with translational constraints along x-axis at the right edge and translational constraints along y-axis at the bottom edge. The analytical solution to the stresses of the quarter plate can be given as:

$$\begin{aligned}
\sigma_{xx}(r,\theta) &= \frac{\sigma_0}{2}\left(2+\frac{3R^4}{r^4}\cos 4\theta-\frac{R^2}{r^2}\left(3\cos 2\theta+2\cos 4\theta\right)\right),\\
\sigma_{yy}(r,\theta) &= \frac{\sigma_0}{2}\left(-\frac{3R^4}{r^4}\cos 4\theta-\frac{R^2}{r^2}\left(\cos 2\theta-2\cos 4\theta\right)\right),\\
\sigma_{xy}(r,\theta) &= \frac{\sigma_0}{2}\left(\frac{3R^4}{r^4}\sin 4\theta-\frac{R^2}{r^2}\left(\sin 2\theta+2\sin 4\theta\right)\right)
\end{aligned} \tag{5}$$

where the magnitude of constant tension (on the infinite boundary) is denoted as σ_0 . A shown in Fig.5, the exact center is the origin of polar coordinates. *R* and *L* are the hole radius and finite quarter plate length, respectively. Regarding material properties, the Youngs modulus *E*, Poisson ratio *v,* and thickness *t* of the planar plate are defined using the values presented in Fig.5.

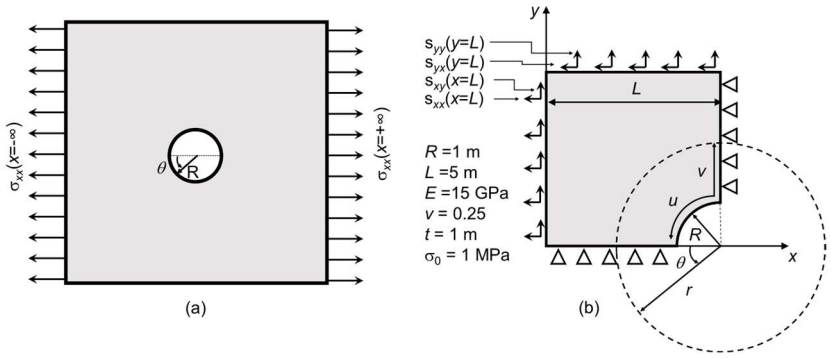

Fig.5 An infinite plate with a circular hole subjected to tension: (a) schematic of the model; (b) a quarter-plate model for analysis

This problem is analysed using the newly developed IGA element (*IGAQuad*) in OpenSEES to evaluate the element performance. The corresponding models of Case 1-6 using order elevation and mesh refinement are illustrated in Fig.6 to show the mesh schemes. For models of Case 1 to Case 3, the basis function order is gradually elevated from 2 to 6 (*k-refinement*), while adopting the same mesh scheme (12×8 elements). The elevation of NURBS order leads to the increasing number of control points from 140 to 308. For Case 4 and 5, the mesh of elements is refined with doubled elements along each axis, while the NUBS order is kept as 2. Moreover, Case 6 adopts an extremely fine mesh, which should provide results sufficiently close to the analytical solution given in Eq.5.

Table 1 IGA models for the infinite plate with circular hole

Case	Order (*u*/*v*)	Control points (*u*/*v*)	Elements (*u*/*v*)
1	2	140 (14/10)	96 (12/8)
2	4	216 (18/12)	96 (12/8)
3	6	308 (22/14)	96 (12/8)
4	2 (doubled elements)	468 (26/18)	384 (24/16)
5	2 (four times elements)	1700 (50/34)	1536 (48/32)
6	2 (Extremely fine mesh)	10004 (122/82)	9600 (120/80)

The distributions of stress σ_{11} (normal stress along x axis) analysed using the IGA models are illustrated in Fig.7, which include the contour plots from Case 1, Case 2 using elevated order and Case 6 using a fine mesh scheme. Except Case 1 of minor differences, Case 2 and Case 6 present nearly identical stress distributions. While the stress distribution of Case 6 is considered as the reference solution, the modelling results of Case 1-5 have shown good

computational performance. Furthermore, the σ_{11} at point A and σ_{22} at point B are retrieved from the models and compared in Fig.8, where the analytical solutions of stresses σ_{11} at A and σ_{22} at B are given as straight lines. In Fig.8, the competitiveness of IGA element is clearly shown in terms of order elevation. While the element order is elevated from 2 to 4 and 6 improving the continuity *from* C^1 to C^5, the error percentage is down to less than 0.1% (Fig.8a). Alternatively, mesh refinement (case 4, 5) can achieve similar accuracy improvement, with the price is the significantly increased number of elements (Fig.8b).

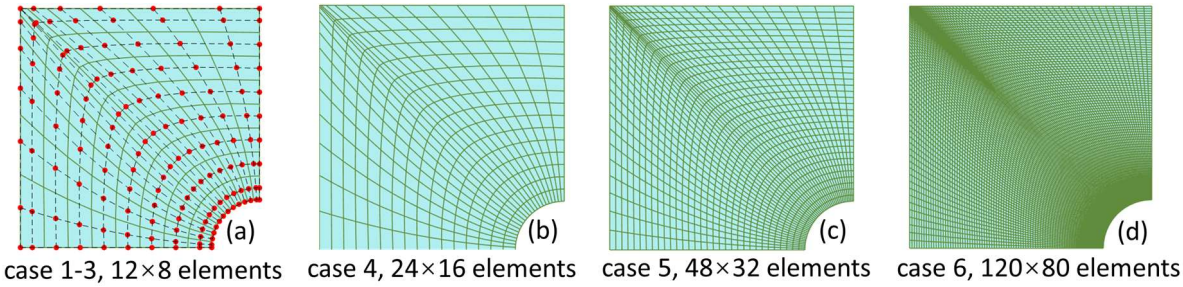

Fig.6 Various mesh schemes for modelling the quarter plate: (a) case 1-3, control points of case 1; (b) case 4; (c) case 5; (d) Case 6 (fine mesh)

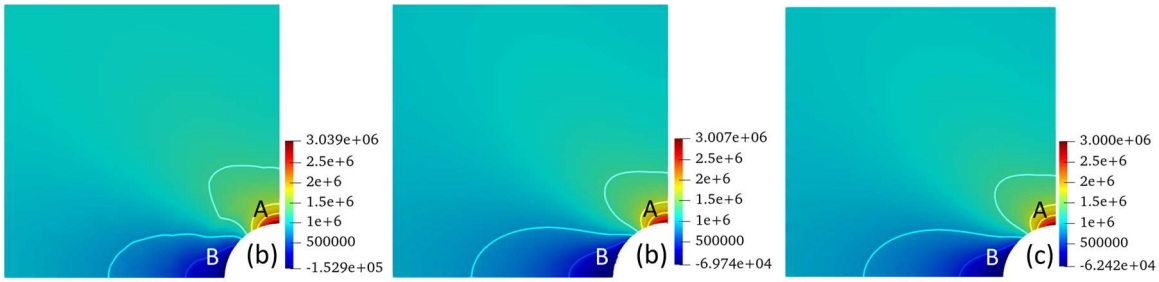

Fig.7 Contour plots of stress σ_{11}: (a) Case 1; (b) Case2 using elevated element order (c) Case 6 using fine mesh as reference

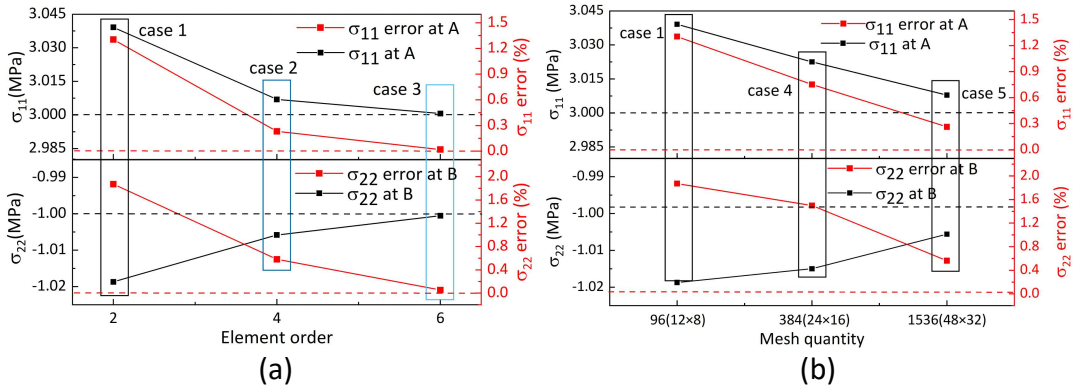

Fig.8 Accuracy of various IGA models: (a) elevated element order; (b) mesh refinement

3.2 3D case: a cylinder with internal pressure

The second benchmark case is to demonstrate the performance of the *IGABrick* element using a 3D case, which models a cylinder with uniform pressure on its internal surface, as shown in Fig.9. A quarter model is built for analyses using IGA elements and FE elements after considering symmetry. Here an FE model of a fine mesh analysed using Abaqus [40] serves as the reference solution for performance comparison. For this 3D model, its geometric parameters, boundary conditions, and loading conditions are illustrated in Fig.9, whereas its material parameters are identically defined as the material model in the 2D plate cases.

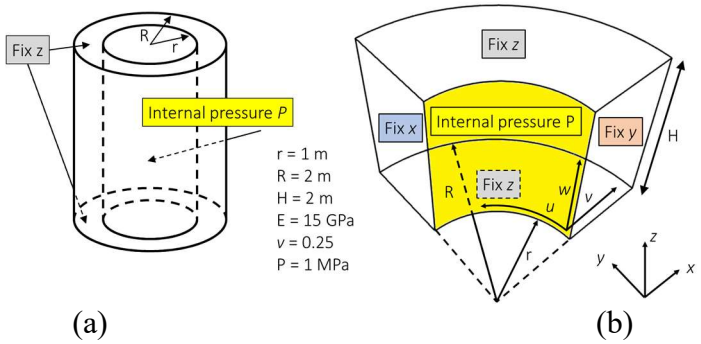

Fig.9 A hollow cylinder with internal pressure: (a) schematic of the model; (b) quarter model for numerical analyses

To examine the computational performance of *IGABrick* element, the models of this 3D cylinder are varied in mesh and NURBS orders. Similarly, the various simulation schemes using the *IGABrick* elements are listed in Table 2. The modelled cases are numbered as four groups: A1~A4, B1~B4, C1~C4, D1~D4. For these groups, the NURBS order has been changed in different directions of u, v, and w (as shown in Table 2) from 2 to 4. In each group, the mesh schemes are changed from a relatively coarse mesh to a fine mesh, which are of two additional elements in all directions as the case number increases. Correspondingly, the number of control points change as a result of elevated order and refined mesh scheme, as shown in the Table 2. Considering that the resolution over the thickness of the cylinder (v-direction) is crucial to the accuracy of analyses, relatively more knots are used than the directions of u and w.

Table 2 Simulation cases for modelling 3D cylinder with different order and mesh schemes

Case	Order (u/v/w)	Control points (u/v/w)	Elements (u/v/w)
A1	2×2×2	96 (4×6×4)	16 (2×4×2)
A2		288(6×8×6)	96 (4×6×4)
A3		640 (8×10×8)	288 (6×8×6)
A4		1200 (10×12×10)	640 (8×10×8)
B1~B4	2×3×2	112~1300 (4~10/7~13/4~10)	16~640 (2~8/4~10/2~8)
C1~C4	2×4×2	128~1400 (4~10/8~14/4~10)	16~640 (2~8/4~10/2~8)
D1~D4	3×3×3	175~1573 (5~11/7~13/5~11)	16~640 (2~8/4~10/2~8)
E1~E4	4×4×4	288~2016 (6~12/8~14/6~12)	16~640 (2~8/4~10/2~8)

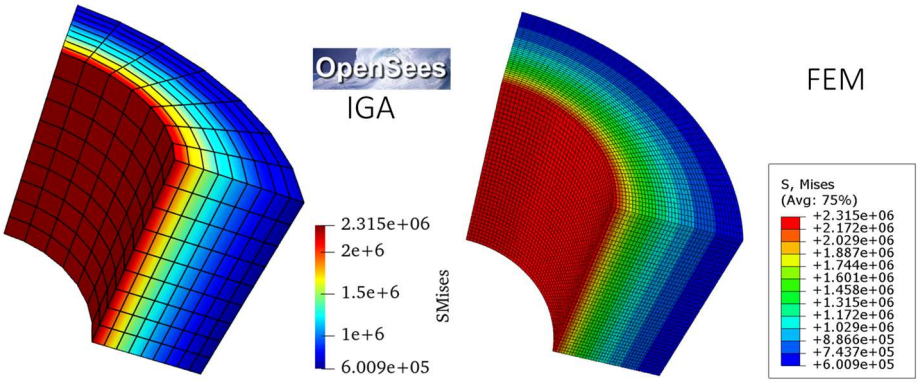

(a) (b)

Fig.10 Mises stress distribution of case E4 and reference FEM case

The reference solution using an FEM model is built with $50 \times 40 \times 40$ isoparametric elements in ABAQUS. As presented in Fig.10, the Mises stress distribution of Case E4 and the reference FEM solution are illustrated as contour plots, which are very close in terms of stress distribution. After retrieving the maximum Mises stresses from the models of all above-mentioned cases, the performance of IGA element in OpenSEES can be observed in Fig.11. With the mesh refinement in A1~A4, the peak stresses quickly approach to the reference solution, which is 2.315 MPa indicated by the dashed line. Moreover, the elevation of NURBS order in case groups of B, C, D and E is significantly more efficient. Even with the least elements (2×4×2 elements), the results have become very close to the reference solution. If comparing the case groups of B and C with the groups of D and E, a lower order over the

directions of u and w causes minor effect on the analysis accuracy. However, increasing the order over thickness direction (v) in the models as shown among the case groups of A, B, and C poses high sensitivity. As demonstrated in the two cases, elevating NURBS order along with a fixed mesh scheme can ultimately facilitate the iterative simulation for OpenSEES-based topology optimization, which favourably alleviates the mesh refinement required by FEM analyses .

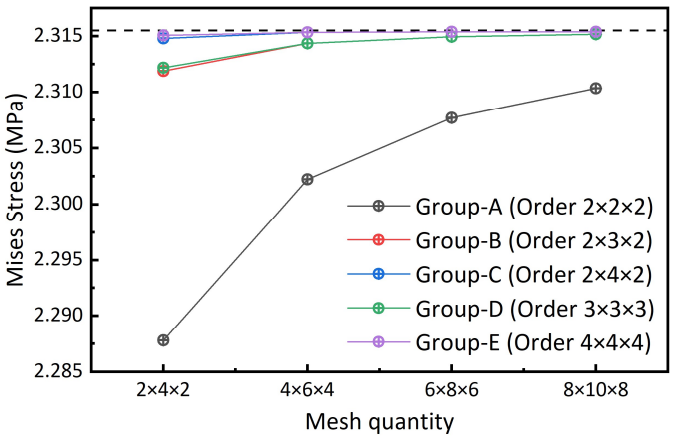

Fig.11 Computational performance of IGABrick elements in modelling a hollow cylinder using various modelling schemes

4. Development of OPS-ITO framework for topology optimization

4.1 OpenSEES-IGA based SIMP method

The Solid Isotropic Material with Penalization (SIMP) method is one of the widely used approaches for topology optimization [41]. This method introduces the elemental or nodal density as the topological design variables, which maintains a simple but efficient mathematical formulation in describing the optimised topology. Furthermore, the introduction of isogeometric analysis into the SIMP-based optimization leads to the Isogeometric Topology Optimization (ITO), which combines the advantages of both methods. In the ITO framework, the elemental stiffness matrix $\mathbf{K}_e$ is expressed as:

$$\begin{aligned}\mathbf{K}_e &= \int_{\Omega_e} \mathbf{B}_e^T \mathbf{D}_e \mathbf{B}_e d\Omega_e \\ \mathbf{D}_e &= \left((1-\rho_{\min})\rho_e^p + \rho_{\min}\right)\mathbf{D}_0\end{aligned} \tag{6}$$

where $\mathbf{B}_e$ is the strain-displacement matrix, and $\mathbf{D}_e$ is the elemental elastic matrix. $\mathbf{D}_e$ is the solid elastic matrix $\mathbf{D}_0$ controlled by the elemental density ρ_e, while p is the penalty coefficient to penalize the intermediate density. Here the minimum density $\rho_{\min}$ is used to avoid numerical instability when ρ_e approaches to zero. Following the same NURBS shape function in Eq.3, the density of element centroid is defined as:

$$\rho_e = \sum_{i=1}^{n}\sum_{j=1}^{m} R_{i,j}^{p,q}\left(\xi_e^c, \eta_e^c\right)\rho_{i,j} \tag{7}$$

The NURBS shape function is based on multiple input variables according to its order and mesh density, which is unlike the shape function of FE analysis limited to the domain of each single element. Since it is a natural density filter, the filter size relies on the order and size of the mesh, which leads to the unfavourable dependency of the filter size on the element sizes (model resolution). There are two major approaches to facilitate independent filter under the ITO framework: (1) to apply an additional distance-based filter[42]; or (2) to apply a multi-resolution approach [43], which uses the different sizes of NURBS shape functions in structural analysis (Eq.3) and in addressing the elemental density (Eq.7). The second approach utilizes the NURBS shape function as a filter, and the first approach is simpler when predicting the minimum length scale of the optimal structure in the context of construction-oriented topology optimization [16] . The distance-based filter is adopted in the present formulation, and the filter is expressed as:

$$\tilde{\rho}_e = \frac{\sum_{j\in N_i} w_{ij}\rho_j}{\sum_{j\in N_i} w_{ij}} \tag{8}$$

Where w_{ij} is a linear distance weighting function given as:

$$w_{ij} = r_{\min} - \left\|\mathbf{x}_j - \mathbf{x}_i\right\| \tag{9}$$

In the above equation, $r_{\min}$ is the filter radius, representing the cartesian distance between the centroid of *i*-th and *j*-th element. ρ_j is the density variable of the *j*-th element.

4.2 Optimization models in ITO tool

In the developed OpenSEES-ITO tool package, it currently supports two typical topology optimization models, a minimum compliance model and a minimum volume (with stress constraints) model [41] . These models are employed to define the objectives of topology optimization, which are briefly explained as below:

(1) Minimum compliance model

The minimum compliance model aims to find the optimal material distribution that minimizes the structural compliance under the prescribed volume ratio. The optimization model is defined as:

$$\begin{aligned} \min_{\boldsymbol{\rho}} \quad & c(\boldsymbol{\rho}) = \mathbf{F}^{\mathrm{T}}\mathbf{U}(\boldsymbol{\rho}) \\ s.t. \quad & \begin{cases} V(\boldsymbol{\rho}) = \sum_e \hat{\rho}_e(\boldsymbol{\rho}) V_e \le \bar{V} \\ \mathbf{K}(\boldsymbol{\rho})\mathbf{U}(\boldsymbol{\rho}) = \mathbf{F} \\ 0 \le \boldsymbol{\rho} \le 1 \end{cases} \end{aligned} \tag{10}$$

Where $\hat{\rho}_e(\boldsymbol{\rho})$ is the projected elemental density by using tanh function [44] to enhance the binarization degree of density variables. The formulation of $\hat{\rho}_e$ is expressed as:

$$\hat{\rho}_e = \frac{\tanh\left(\beta_{HS}\eta_{th}\right) + \tanh\left(\beta_{HS}\left(\tilde{\rho}_e - \eta_{th}\right)\right)}{\tanh\left(\beta_{HS}\eta_{th}\right) + \tanh\left(\beta_{HS}\left(1 - \eta_{th}\right)\right)} \tag{11}$$

The projection is based on the filtered elemental density $\tilde{\rho}_e$ in Eq.8. As the sharpness value β_{HS} increases, the density binarization is strengthened with the threshold η_{th} .

The sensitivity of the volume constraint $V(\boldsymbol{\rho})$ with respect to the design variable control point density can be given as:

$$\frac{\partial V(\boldsymbol{\rho})}{\partial \boldsymbol{\rho}} = \sum_i \frac{\partial V(\boldsymbol{\rho})}{\partial \hat{\rho}_e} \frac{\partial \hat{\rho}_e}{\partial \rho_i} \tag{12}$$

where the term $\frac{\partial \hat{\rho}_e}{\partial \rho_i}$ follows the chain rule, which is sequentially derived from the density filter in Eq.8 and the projection in Eq.11 given as below:

$$\frac{\partial \hat{\rho}_e}{\partial \rho_i} = \frac{\partial \hat{\rho}_e}{\partial \tilde{\rho}_e} \frac{\partial \tilde{\rho}_e}{\partial \rho_e} \frac{\partial \rho_e}{\partial \rho_i} \tag{13}$$

The sensitivity of compliance objective $c(\boldsymbol{\rho})$ is:

$$\frac{\partial c(\boldsymbol{\rho})}{\partial \rho_i} = \sum_e \mathbf{U}_e^T \frac{\partial \mathbf{K}_e}{\partial \rho_i} \mathbf{U}_e \tag{14}$$

where the term $\frac{\partial \mathbf{K}_e}{\partial \rho_i} = \frac{\partial \mathbf{K}_e}{\partial \hat{\rho}_e} \frac{\partial \hat{\rho}_e}{\partial \rho_i}$ is derived by Eq.6 and Eq.13.

(2) Minimum volume model with stress constraint

The minimum volume model is used to find the lightweight structure under prescribed Mises stress constraints to ensure structural safety and resilience. This optimization model can be described as:

$$\begin{aligned} \min_{\boldsymbol{\rho}} \quad & V(\boldsymbol{\rho}) = \sum_e \hat{\rho}_e(\boldsymbol{\rho}) V_e \\ s.t. \quad & \begin{cases} \sigma_{e,i}^M(\boldsymbol{\rho}) \le \bar{\sigma}, \quad 0 \le i \le N_{GP} \\ \mathbf{K}(\boldsymbol{\rho})\mathbf{U}(\boldsymbol{\rho}) = \mathbf{F} \\ 0 \le \boldsymbol{\rho} \le 1 \end{cases} \end{aligned} \tag{15}$$

where the Mises stress at each gauss point $\sigma_{e,i}^M(\boldsymbol{\rho})$ is constrained below the stress limit $\bar{\sigma}$. For the sake of formulation simplicity, the density at elemental center is taken as the density of all corresponding gauss points. To interpolate the stress value of the intermediate density variable and tackle the stress singularity issue, the q-p stress relaxation scheme as suggested in [45] is applied. Therefore, the penalized Mises stress is expressed as:

$$\begin{aligned} & \sigma_{e,i}^M = \left(\boldsymbol{\sigma}_{e,i}^T \mathbf{V} \boldsymbol{\sigma}_{e,i}\right)^{\frac{1}{2}} \\ & \mathbf{V} = \begin{bmatrix} 1 & -1/2 & 0 \\ -1/2 & 1 & 0 \\ 0 & 0 & 3 \end{bmatrix} \\ & \boldsymbol{\sigma}_{e,i} = \hat{\rho}_e^s \mathbf{D}_0 \mathbf{B}_{e,i} \mathbf{u}_e \end{aligned} \tag{16}$$

where $\mathbf{B}_{e,i}$ is the strain-displacement matrix at the *i*-th gauss point of the element. Likewise, the Drucker-Prager stress is also supported to enable unequal tension-compression stress limit, the formulation is available from our former paper[16].

Another challenge is the high computational cost induced by a large number of local stress constraints, which can be reduced using Kreisselmeier-Steinhauser(K-S) or p-norm [46-48] function to aggregate all local constraints as a single global constraint. The K-S function is here applied considering convenient development of future optimization models:

$$G_{KS}\left(\boldsymbol{\rho}\right)=\frac{1}{\eta}\ln\sum_{e}^{N_{GP}}\sum_{i}\exp\left(\eta\frac{\sigma_{e,i}^{M}}{\bar{\sigma}}\right)\le 1 \tag{17}$$

where the aggregation factor η is a positive value, which is to penalize the violated local constraints. A higher η helps to reduce the approximation error of stress measurement but bringing higher nonlinearity and convergence difficulty. To scale the approximation to a reasonable level, an adaptive constraint scaling (ACS) scheme [49] is adopted. It offers more accurate stress measurement with relatively low factor and it also stabilizes the iteration process. The ACS-corrected stress evaluation is described as:

$$\begin{aligned}&\tilde{G}_{KS}^{(I)}\approx c_{ACS}^{(I)}G_{KS}^{(I)}\\&c_{ACS}^{(I)}=\begin{cases}\dfrac{\sigma_{\max}^{(I)}}{G_{KS}^{(I)}}, & I\le 2\\ \dfrac{\sigma_{\max}^{(I-1)}}{\alpha_{ACS}^{(I)}G_{KS}^{(I-1)}}+\left(1-\alpha_{ACS}^{(I)}\right)c_{ACS}^{(I-1)}, & I>2\end{cases}\end{aligned} \tag{18}$$

Where the ACS factor $c_{ACS}^{(I)}$ at *I*-th iteration is weighted by the stress measurement of past iterations, and the weight factor $\alpha_{ACS}^{(I)}$ is suggested as constant 0.5 after 2 initial iterations. As pointed out by Le et al. [49], this weighted ACS factor converges at a constant throughout the iteration, and the influence is gradually reduced to the optimum.

The sensitivity of volume constraint presented in Eq.12, which is along with the adjoint method for the stress constraint sensitivity analysis:

$$\phi(\boldsymbol{\rho}) = G_{KS}(\boldsymbol{\rho}) + \boldsymbol{\lambda}^{\mathrm{T}}\left(\mathbf{K}(\boldsymbol{\rho})\mathbf{U}(\boldsymbol{\rho}) - \mathbf{F}\right) \tag{19}$$

where the adjoint vector $\boldsymbol{\lambda}$ is arbitrary, and the adjoint formulation sensitivity is given by the chain rule:

$$\frac{\partial \phi(\boldsymbol{\rho})}{\partial \rho_i} = \sum_e \sum_i^{N_{GP}} \frac{\partial G_{KS}(\boldsymbol{\rho})}{\partial \sigma_{e,i}^M} \left(\begin{array}{l} \dfrac{\partial \sigma_{e,i}^M}{\partial \hat{\rho}_e} \dfrac{\partial \hat{\rho}_e}{\partial \rho_i} \\ + \dfrac{\partial \sigma_{e,i}^M}{\partial \mathbf{u}_e} \dfrac{\partial \mathbf{u}_e}{\partial \rho_i} \end{array} \right) + \boldsymbol{\lambda}^{\mathrm{T}} \left(\frac{\partial \mathbf{K}}{\partial \rho_i}\mathbf{U} + \mathbf{K}\frac{\partial \mathbf{U}}{\partial \rho_i} \right) \tag{20}$$

To eliminate the component with the implicit term $\dfrac{\partial \mathbf{u}_e}{\partial \rho_i}$, a specific adjoint vector $\boldsymbol{\lambda}$ is solved by:

$$\frac{\partial G_{KS}(\boldsymbol{\rho})}{\partial \sigma_{e,i}^M} \frac{\partial \sigma_{e,i}^M}{\partial \mathbf{u}_e} + \boldsymbol{\lambda}^{\mathrm{T}}\mathbf{K} = 0 \tag{21}$$

where the term $\dfrac{\partial G_{KS}(\boldsymbol{\rho})}{\partial \sigma_{e,i}^M}$ is the sensitivity of K-S aggregation in Eq.18. $\dfrac{\partial \sigma_{e,i}^M}{\partial \hat{\rho}_e}$ and $\dfrac{\partial \sigma_{e,i}^M}{\partial \mathbf{u}_e}$ are from Eq.16.

4.3 Development of ITO tool for OPS-ITO framework

Based on OpenSEES-IGA and SIMP formulation, an ITO tool with graphical user interface has been developed to perform topology optimization with the developed IGA in OpenSEES. As depicted in Fig.12, the OPS-ITO tool package comprises three modules: (1) ITO tool: A toolset with graphical user interface (GUI) embedding the middleware and interface ported to the analysis module and TO module. The GUI provides entry for defining the model geometry, mesh and boundary conditions to be used in OPS-IGA and the optimization parameters for TO iterations. For visualisation after the optimization procedure, a middleware is established to export jpg/vtk files for 2D and 3D models to support the display of displacements, strains, and stresses. (2) OPS-IGA Module: When receiving OpenSEES input file (*Tcl* or *Python* script), the simulation model will be created in OpenSEES using the corresponding IGA elements (*IGAQuad* or *IGABrick*). In each iteration, the results from the completed analysis will be recorded using nodal and elemental recorders and transferred to the

TO module and GUI. (3) TO module: It is responsible to performing topology optimization with various sensitivity functions for different optimization goals, such as minimum compliance, minimum volume with material strength, the pattern compliance to control number of variations, and other constraint functions of potential interest. Density of control points are generated from the TO procedures and transferred to the IGA models for iterative analyses.

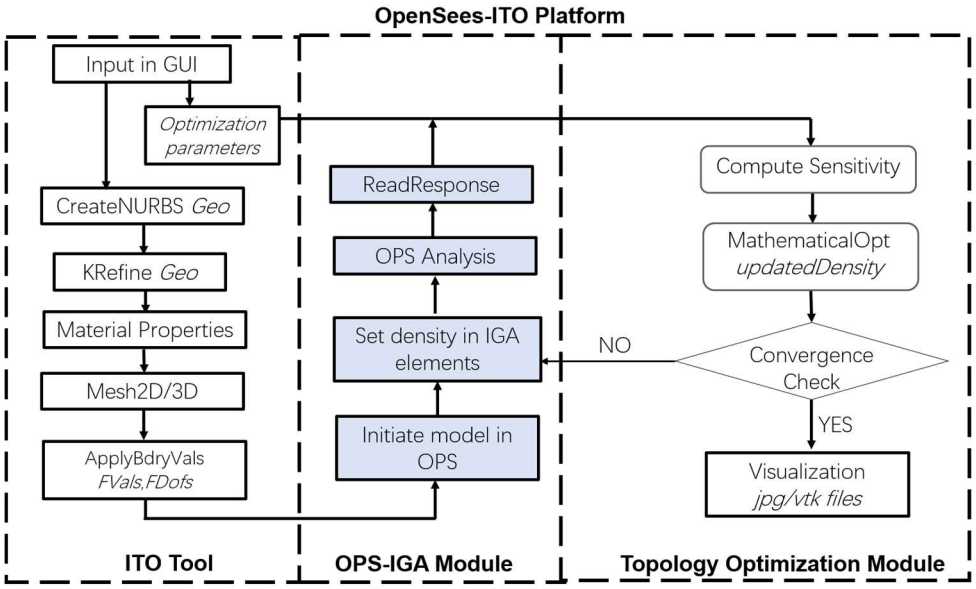

Fig.12 OPS-ITO framework comprising model setup, IGA analysis, and optimization module

4.4 Graphical user interface for OPS-ITO framework

The OPS-ITO framework has been packed as a tool package and can be executed using an executable program with GUI, which is illustrated in Fig.13. The currently available input parameters are listed in Fig.13a~c, while the model visualizations are set up in Fig.13d~e. It presents the real-time topology configuration, and the iterative histories of objective index and constraints. 2D and 3D problems have been enabled, which allows optimization using the typical optimization models as *minCompliance* (compliance minimization with volume constraint) and *minVolume* (volume minimization with Mises stress constraint).

To launch the optimization analysis, the input parameters are required as three categories: (a) model dimension, optimization type, and geometric model, (b) material, boundary, and load conditions, and (c) optimization parameters. After setting the 2D/3D option and optimization

type option, the model geometry can be defined for two types of models: (1) Simple models: Frequently used rectangular or brick types of initial design space can be activated '*Default*', which allows users to define the size of the rectangular or boxy design space, element number and orders of each direction. (2) Complex models: The option '*User input*' can be chosen for models of irregular design space using the pre-process of SIMOPackage [39] as introduced before. The information of generated geometric model is stored as the *Surf/Volu* variables saved as a Matlab file (.mat), which can be imported by the OPS-ITO executable.

The material definition of the model takes advantage of the extensive collection of materials in OpenSEES as an open source simulation platform. Currently the isotropic linear elastic material is used as a default material, which can be further extended by co-working with the OpenSEES isogeometric analyses. Moreover, the definition of loading and boundary conditions can be conducted using the pre-process tool of the SIMOPackage. Additional definitions of loading or boundary condition is allowed on the user interface using a script line comprising a boundary index, a type label, and a distribution expression. The typical face indices of 2D and 3D models are presented in Fig.14. The type label allows *UX, UY, UZ* for boundary conditions and *FX, FY, FZ, PRESS* for load conditions, and the 2D/3D function handle expression begins with @(x,y)/@(x,y,z).

As shown in Fig.13, the category of (c) OptParameters defines various parameters for topology optimization process, which are corresponding to the previously mentioned target constraint functions. The *ConstValue* (volume limit $\bar{V}$ in Eq.10 or Mises stress limit $\bar{\sigma}$ in Eq.15) indicates the maximum value of constraint, while the maximum number of iterations is given as *MaxIter*. *MMAMoveLimits* sets the move limit of MMA optimization algorithm, and *Penalty* indicates the density penalty order of SIMP method. *Projection* (β_{HS}) is the sharpness value of the erode/dilate Heaviside function, which determines the 0-1 solution degree of optimized topology configuration, and the projection threshold is set by *ProjThreshold* (η_{th}). To

accelerate the convergence and optimal topology generation, the stepped penalty and projection can be respectively activated by *StpPenalty* and *StpProj*, these two parameters default raise 1 per 10 iterations, the function of the minimum component size scale is controlled by *r_min* (r_{min}) to avoid possible over-thin components and improve the constructability.

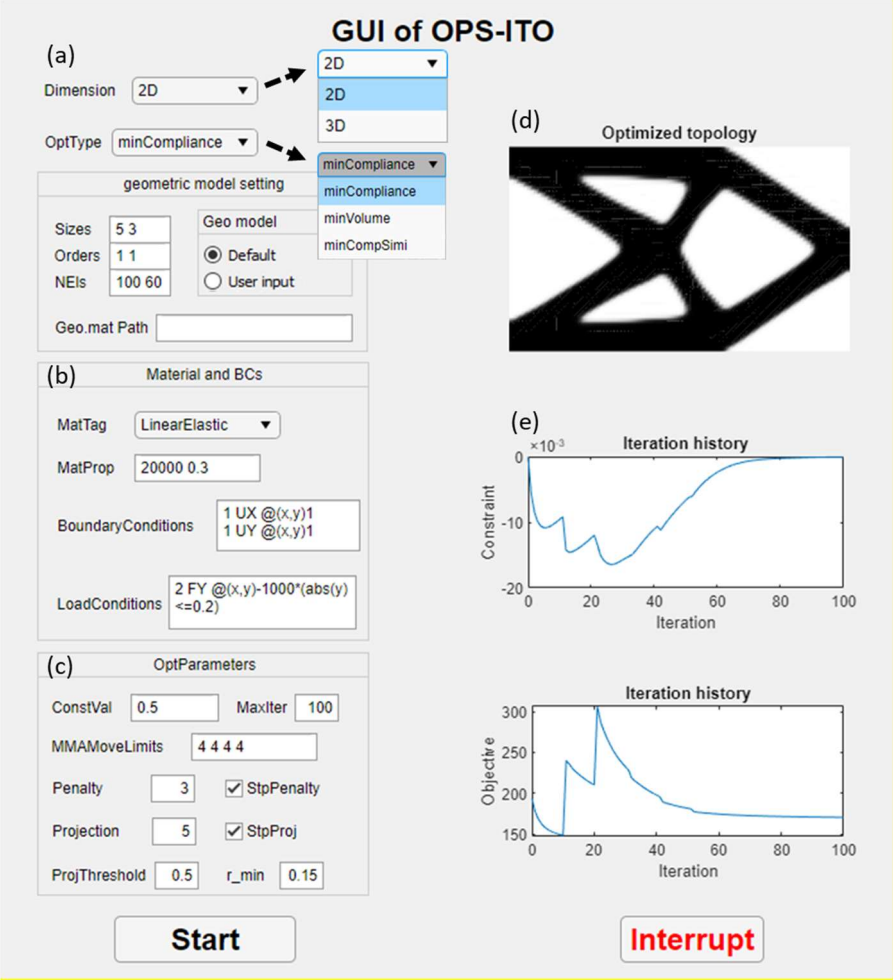

Fig.13 Graphical user interface of OPS-ITO platform

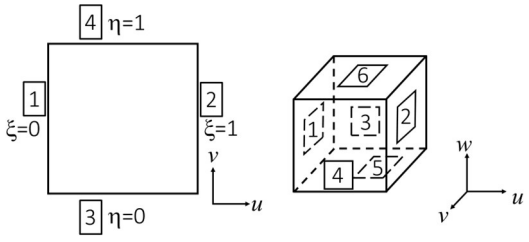

Fig.14 Illustration of elemental boundary indexes (boxed): (a) 2D model; (b) 3D model

5. Demonstration of using OPS-ITO framework

To demonstrate the use of OPS-ITO framework for structural design optimization, four cases have been conducted and briefly described regarding the different optimization schemes. An L-shape beam is optimized for minimum volume ratio under various stress constraints of structural materials, followed by a 3D cantilever beam case to showcase the 3D optimization under minimum compliance, i.e., the stiffest beam with a prescribed volume ratio. The last case is to show the optimization of a structural system reflecting a long-term vision, which considers the pattern compliance regarding the manufacturability and aesthetic performance.

5.1 A 2D L-shape beam optimized for minimum volume with strength limits

Strength limits of construction materials are practical concern for real structural design, which shall be included in the OPS-ITO package. An L-shape beam is modelled for demonstration of this purpose, which is fixed at the top edge with a downward load of 250 kN at the free end as shown in Fig.15. The initial design domain of this L-shape is defined by using the *SIMOPackage* by giving a readable file through *'User input'* option in the GUI, which contains the *Surf* variables of the model. For the optimization parameters, lower MMA move limits and a higher maximum of iteration number 300 are adopted since the stress constraint of structural material introduces difficulties to the convergence. The filter size is reduced to 0.01 to allow for slightly slimer components with high-stress level. The input parameters for GUI are listed in Table 3.

Regarding the stress constraint, the Mises and Drucker-Prager strength limits are applied separately to this L-shape beam, which are usually suitable for steel sections and concrete sections (including fiber reinforced concrete), respectively. The K-S aggregation factor is default set as 8, and the Mises stress state is corrected by the ACS method in Eq.19. The stress contour plots are shown in Fig.15, where the effect of imposing Mises strength limit is shown in Fig.15a and the effect of imposing Drucker-Prager strength limit is given in Fig.15b. The contour plots represent the ratios of corresponding stress terms over the assigned strengths,

which are iteratively changing as a result of model. For a concrete type of material of different strengths for tension and compression, the eventual topology of the L-shape beam requires stronger components in tension region. This strength limit enabled in topology optimization can be later applied for designs of real 3D printable structures, only requiring the corresponding material properties [50] prior to the design.

Table 3. Input parameters for optimization of a L-shape beam

Parameter name	Value	Parameter name	Value
Geo model	User input	Geo.mat Path	stressCase.mat
MatTag	ElasticIsotropic	MatProp	4e10 0.3
BCs	1 UX @(x,y)1 1 UY @(x,y)1	Loads	4 FY @(x,y)-5e6*(x>=1.95)
ConstVal	10e6	MaxIter	400
MMAPars	1 0.5 0.5 1	Penalty	3
StpPenalty	×	Projection	0.1
StpPrj	×	ProjThreshold	0.5
rmin	0.01		

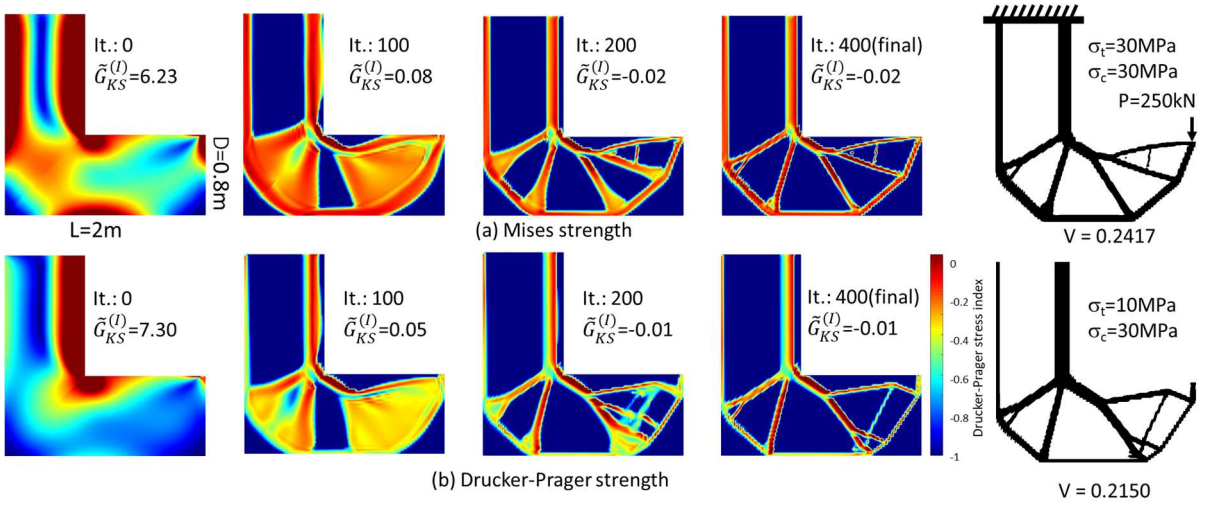

Fig.15 Optimization of L-shape beam for light weight under strength constraints: (a) using Mises stress constraint; (b) using Drucker-Prager stress constraint

5.2 A cantilever beam optimized in 3D domain

In addition to the 2D planar cantilever beam that is widely optimized, it can be either optimized regarding a 3D domain using IGABrick elements and the OPS-ITO platform. This further alleviates the constraint along the thickness direction during the optimization iterations. The *minCompliance* module for a 3D domain is employed using the boundary conditions and

material properties identical to the 2D beam except the thickness of 1 m. The input parameters of this 3D cantilever beam are listed in Table 4.

Table 4 Input parameters for optimization of 3D cantilever beams

Parameter name	Value	Parameter name	Value
Geo model	Default	Sizes	5 3 1
Orders	1 1 1	NEls	30 18 6
MatTag	ElasticIsotropic	MatProp	2e11 0.3
BCs	1 UX @(x,y,z)1 1 UY @(x,y,z)1 1 UZ @(x,y,z)1	Loads	2 FY @(x,y,z)- 1e5*(abs(y)<=0.05) *(abs(z-0.5)<=0.05)
ConstVal	0.3	MaxIter	100
MMAPars	4 2 2 4	Penalty	5
StpPenalty	√	Projection	5
ProjThreshold	0.5	ProjThreshold	0.5
rmin	0.3		

In Fig.16, the variations of beam topology are shown alongside the iteration tags. Both the beams are subjected to 100kN/m^2 force on an area of 0.1m×0.1m at one end, while the other end of each beam is fixed. When the optimization iteration proceeds, the rendering of beam topology gradually becomes crisp from the initially gloomy topology. Noted the shape visualization using Paraview for these optimized models have been internally smoothed as interpolated contour. In Fig.16a, the initial beam is prescribed as a rectangular shape. The volume ratio converges to 0.3 after the first 20 iterations, which is accompanied by the compliance index reducing to 2.18N*mm upon the completion of 100 iterations as illustrated. In Fig.16b, the initial geometry of the cantilever beam is of a curved shape (a quarter of 1m radius circle), and its thickness is prescribed as 0.5m. Compared to the 2D topology, hollow sections and voids are seen inside the beam, and the beam behaviour will be similar to a space truss. Obviously, 3D printing construction is more suitable for this type of beam design after optimization. This enables the most efficient use of construction materials and it would potentially reduce the carbon footprint at the construction stage, especially when this technique

is combined with the use of other sustainable structural materials in the era of pursuing carbon neutrality.

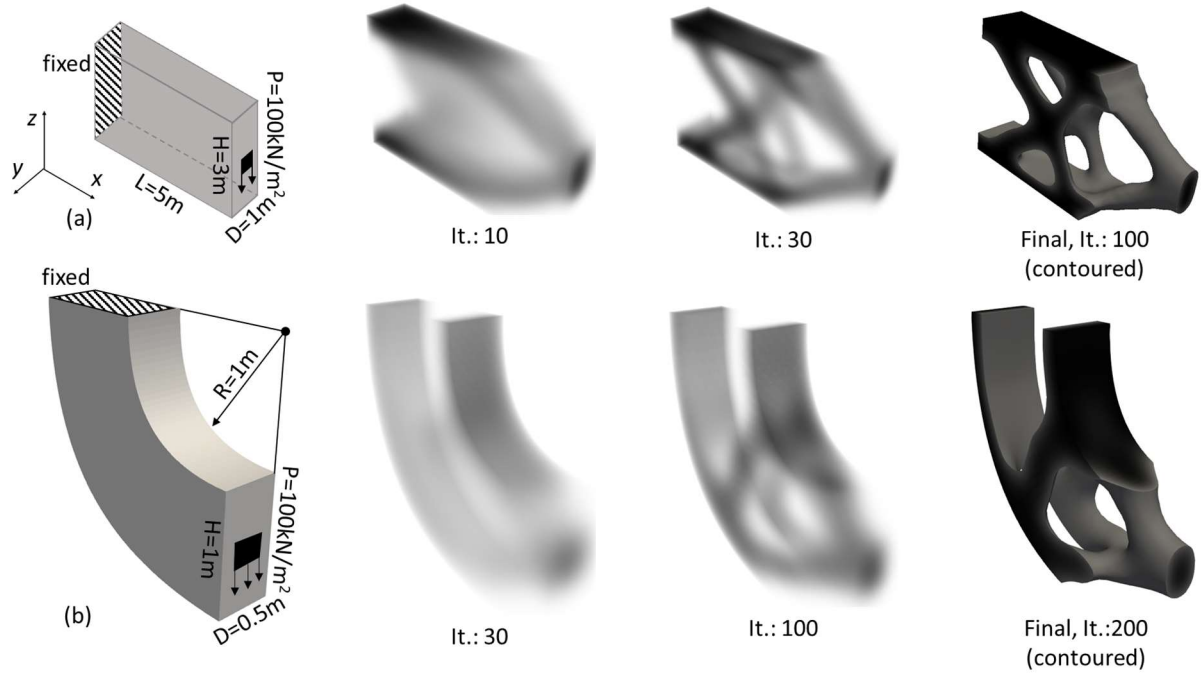

Fig.16 Optimization of 3D cantilever beams: (a) a rectangular beam; (b) a curved beam

6. Conclusion

In this paper, an OPS-ITO platform has been established, which employs IGA elements to perform analyses of structural members or structural systems for the iteration of topology optimization. The SIMP-based optimization is developed and conducted in this OPS-ITO framework, which is able to find optimal distribution of materials in a design domain aiming for minimum volume or minimum compliance with the consideration of material strength limits. The OPS-ITO tool package reflects the authors' vision of future building design, which first ever attempts to provide a design tool to resolve the need as the structure is unnecessarily designed with conventionally regular shapes. The work presented in this paper can be summarized as follows:

(1) The IGA elements for 2D and 3D structural analyses have been developed in the open-source simulation platform OpenSees, which uses NURBS for geometric description and shape

functions in element state determination. NURBS as the basis of computer-aided design, provides seamless solution from model geometry to numerical description.

(2) The outstanding performance of IGA elements has been demonstrated using 2D and 3D benchmark studies. IGA models can achieve accurate results by simply elevating NURBS order rather than the traditional mesh refinement.

(3) An OPS-ITO tool is developed to integrate the graphic user interface, pre-processing, OPS-IGA modelling, and optimization process. Standard 2D or 3D minimum compliance model and minimum volume model with stress constraints have been developed as optimization objective and constraint functions. The optimized geometric model can be exported for further post-processing or 3D printing.

(4) Three case studies of using OPS-ITO package are discussed, including the optimization of beams in 2D and 3D domains, an L-shape beam with Mises and Drucker-Prager strength limits.

(5) The OPS-ITO package is a simulation platform for topology optimization based structural design, which generates optimal designs of free-form geometries suitable for future structural construction. The open-source and module-based code framework of OpenSees will facilitate continuous development of various objective and constraint functions to fulfil the performance needs of modern and future structures.

Acknowledgments

The authors would like to acknowledge the financial support of the RISUD Ph.D. studentship to first author Zixin Zhang and the Hong Kong Polytechnic University Ph.D. studentship to Tejeswar Yarlagadda. The financial support from the PolyU startup fund (P0031564) and the RIAM fund are gratefully acknowledged.

Declaration of competing interest

The authors declare that no conflict of interest is encountered in this paper.

References

[1] S.C. Paul, G.P. van Zijl, M.J. Tan, I. Gibson, A review of 3D concrete printing systems and materials properties: Current status and future research prospects, Rapid Prototyping Journal, 24 (2018) 784-798.

[2] Z. Chang, Y. Xu, Y. Chen, Y. Gan, E. Schlangen, B. Šavija, A discrete lattice model for assessment of buildability performance of 3D-printed concrete, Computer-Aided Civil and Infrastructure Engineering, 36 (2021) 638-655.

[3] Y. Xia, M. Langelaar, M.A. Hendriks, A critical evaluation of topology optimization results for strut-and-tie modeling of reinforced concrete, Computer-Aided Civil and Infrastructure Engineering, 35 (2020) 850-869.

[4] X. Zhang, Y.M. Xie, S. Zhou, A nodal-based evolutionary optimization algorithm for frame structures, Computer-Aided Civil and Infrastructure Engineering, (2022).

[5] O.C. Zienkiewicz, R.L. Taylor, P. Nithiarasu, J. Zhu, The finite element method, McGraw-hill London, 1977.

[6] M.P. Bendsøe, O. Sigmund, Material interpolation schemes in topology optimization, Archive of Applied Mechanics, 69 (1999) 635-654.

[7] M.P. Bendsoe, O. Sigmund, Topology optimization: theory, methods, and applications, Springer Science & Business Media, 2003.

[8] T. Yarlagadda, Z. Zhang, L. Jiang, P. Bhargava, A. Usmani, Solid isotropic material with thickness penalization–A 2.5 D method for structural topology optimization, Computers & Structures, 270 (2022) 106857.

[9] N.P. van Dijk, K. Maute, M. Langelaar, F. Van Keulen, Level-set methods for structural topology optimization: a review, Structural and Multidisciplinary Optimization, 48 (2013) 437-472.

[10] X. Guo, W. Zhang, W. Zhong, Doing topology optimization explicitly and geometrically—a new moving morphable components based framework, Journal of Applied Mechanics, 81 (2014).

[11] A.N. Christiansen, M. Nobel-Jørgensen, N. Aage, O. Sigmund, J.A. Bærentzen, Topology optimization using an explicit interface representation, Structural and Multidisciplinary Optimization, 49 (2014) 387-399.

[12] H. Lian, A.N. Christiansen, D.A. Tortorelli, O. Sigmund, N. Aage, Combined shape and topology optimization for minimization of maximal von Mises stress, Structural and Multidisciplinary Optimization, 55 (2017) 1541-1557.

[13] O. Amir, A topology optimization procedure for reinforced concrete structures, Computers & Structures, 114 (2013) 46-58.

[14] J. Liu, Y. Ma, A survey of manufacturing oriented topology optimization methods, Advances in Engineering Software, 100 (2016) 161-175.

[15] L.L. Beghini, A. Beghini, N. Katz, W.F. Baker, G.H. Paulino, Connecting architecture and engineering through structural topology optimization, Engineering Structures, 59 (2014) 716-726.

[16] Z. Zhang, T. Yarlagadda, Y. Zheng, L. Jiang, A. Usmani, Isogeometric analysis-based design of post-tensioned concrete beam towards construction-oriented topology optimization, Structural and Multidisciplinary Optimization, 64 (2021) 4237-4253.

[17] Y. Lai, Y.J. Zhang, L. Liu, X. Wei, E. Fang, J. Lua, Integrating CAD with Abaqus: a practical isogeometric analysis software platform for industrial applications, Computers & Mathematics with Applications, 74 (2017) 1648-1660.
[18] J. Gao, L. Gao, Z. Luo, P. Li, Isogeometric topology optimization for continuum structures using density distribution function, International Journal for Numerical Methods in Engineering, 119 (2019) 991-1017.
[19] T.J. Hughes, J.A. Cottrell, Y. Bazilevs, Isogeometric analysis: CAD, finite elements, NURBS, exact geometry and mesh refinement, Computer Methods in Applied Mechanics and Engineering, 194 (2005) 4135-4195.
[20] Y. Wang, Z. Wang, Z. Xia, L.H. Poh, Structural design optimization using isogeometric analysis: a comprehensive review, Computer Modeling in Engineering & Sciences, 117 (2018) 455-507.
[21] V.P. Nguyen, C. Anitescu, S.P. Bordas, T. Rabczuk, Isogeometric analysis: an overview and computer implementation aspects, Mathematics and Computers in Simulation, 117 (2015) 89-116.
[22] H. Liu, D. Yang, P. Hao, X. Zhu, Isogeometric analysis based topology optimization design with global stress constraint, Computer Methods in Applied Mechanics and Engineering, 342 (2018) 625-652.
[23] D. Benson, Y. Bazilevs, M.-C. Hsu, T. Hughes, Isogeometric shell analysis: the Reissner–Mindlin shell, Computer Methods in Applied Mechanics and Engineering, 199 (2010) 276-289.
[24] J. Gao, M. Xiao, Y. Zhang, L. Gao, A comprehensive review of isogeometric topology optimization: methods, applications and prospects, Chinese Journal of Mechanical Engineering, 33 (2020) 1-14.
[25] J. Gao, L. Wang, Z. Luo, L. Gao, IgaTop: an implementation of topology optimization for structures using IGA in MATLAB, Structural and Multidisciplinary Optimization, 64 (2021) 1669-1700.
[26] F. McKenna, OpenSees: a framework for earthquake engineering simulation, Computing in Science & Engineering, 13 (2011) 58-66.
[27] B. Patzák, OOFEM—an object-oriented simulation tool for advanced modeling of materials and structures, Acta Polytechnica, 52 (2012).
[28] J.K. Ousterhout, Tcl: An embeddable command language, Citeseer, 1989.
[29] M. Zhu, M.H. Scott, Modeling fluid–structure interaction by the particle finite element method in OpenSees, Computers & Structures, 132 (2014) 12-21.
[30] X. Lu, L. Xie, H. Guan, Y. Huang, X. Lu, A shear wall element for nonlinear seismic analysis of super-tall buildings using OpenSees, Finite Elements in Analysis and Design, 98 (2015) 14-25.
[31] N.M. Noh, L. Liberatore, F. Mollaioli, S. Tesfamariam, Modelling of masonry infilled RC frames subjected to cyclic loads: State of the art review and modelling with OpenSees, Engineering Structures, 150 (2017) 599-621.
[32] J. Jiang, A. Usmani, G.-Q. Li, Modelling of steel-concrete composite structures in fire using OpenSees, Advances in Structural Engineering, 17 (2014) 249-264.
[33] L. Jiang, Y. Jiang, Z. Zhang, A. Usmani, Thermal analysis infrastructure in OpenSees for fire and its smart application interface towards natural fire modelling, Fire Technology, (2021) 1-26.
[34] L. Jiang, A. Usmani, Computational performance of beam-column elements in modelling structural members subjected to localised fire, Engineering Structures, 156 (2018) 490-502.
[35] L. Jiang, A. Usmani, Towards scenario fires–modelling structural response to fire using an integrated computational tool, Advances in Structural Engineering, 21 (2018) 2056-2067.
[36] L. Piegl, W. Tiller, The NURBS book, Springer Science & Business Media, 1996.

[37] Y.-D. Seo, H.-J. Kim, S.-K. Youn, Isogeometric topology optimization using trimmed spline surfaces, Computer Methods in Applied Mechanics and Engineering, 199 (2010) 3270-3296.
[38] R.N. Simpson, S.P. Bordas, H. Lian, J. Trevelyan, An isogeometric boundary element method for elastostatic analysis: 2D implementation aspects, Computers & Structures, 118 (2013) 2-12.
[39] SIMOGroup, SIMO-Package, a basic NUBS-based IsoGeometric Analysis package written in MATLAB, https://github.com/SIMOGroup/SIMO-Package, 2016.
[40] G. Abaqus, Abaqus 6.11, Dassault Systemes Simulia Corporation, Providence, RI, USA, (2011).
[41] O. Sigmund, K. Maute, Topology optimization approaches, Structural and Multidisciplinary Optimization, 48 (2013) 1031-1055.
[42] J.K. Guest, J.H. Prévost, T. Belytschko, Achieving minimum length scale in topology optimization using nodal design variables and projection functions, International Journal for Numerical Methods in Engineering, 61 (2004) 238-254.
[43] G. Costa, M. Montemurro, J. Pailhès, Minimum length scale control in a NURBS-based SIMP method, Computer Methods in Applied Mechanics and Engineering, 354 (2019) 963-989.
[44] B.S. Lazarov, F. Wang, O. Sigmund, Length scale and manufacturability in density-based topology optimization, Archive of Applied Mechanics, 86 (2016) 189-218.
[45] P. Duysinx, M.P. Bendsøe, Topology optimization of continuum structures with local stress constraints, International Journal for Numerical Methods in Engineering, 43 (1998) 1453-1478.
[46] P. Duysinx, O. Sigmund, New developments in handling stress constraints in optimal material distribution, in: 7th AIAA/USAF/NASA/ISSMO symposium on multidisciplinary analysis and optimization, 1998, pp. 4906.
[47] R. Yang, C. Chen, Stress-based topology optimization, Structural Optimization, 12 (1996) 98-105.
[48] A. Verbart, M. Langelaar, F. Van Keulen, A unified aggregation and relaxation approach for stress-constrained topology optimization, Structural and Multidisciplinary Optimization, 55 (2017) 663-679.
[49] C. Le, J. Norato, T. Bruns, C. Ha, D. Tortorelli, Stress-based topology optimization for continua, Structural and Multidisciplinary Optimization, 41 (2010) 605-620.
[50] N. Stoiber, B. Kromoser, Topology optimization in concrete construction: a systematic review on numerical and experimental investigations, Structural and Multidisciplinary Optimization, 64 (2021) 1725-1749.